ARTICLE OPEN

Check for updates

# Highly sensitive active-powering pressure sensor enabled by integration of double-rough surface hydrogel and flexible batteries

Yuan Huang[1,6], Binbin Liu[2,6], Wenyue Zhang[3], Gangrui Qu[2], Shunyu Jin[4], Xianbo Li[3], Zanxiang Nie[5] and Hang Zhou[2]✉

A conductive, elastic, and biocompatible hybrid network hydrogel was prepared by cross-linking of locust bean gum, polyvinyl alcohol, and carbon nanotubes, yielding a rough top surface and smooth bottom surface. The merging of the two pieces of hydrogel flat face to flat face forms a highly elastic hydrogel with double-rough surfaces. A piezoresistive sensor assembled with the double-rough surface hydrogel sandwiched between two carbon cloth electrodes exhibits a high sensitivity (20.5 kPa-1, 0-1kPa), a broad detection range (0.1–100 kPa) and a reliable response for 1000 cycles. The rough contact area between the hydrogels and the carbon cloth is found critical in achieving ultra-high sensitivities in the low-pressure range. Moreover, further monolithic integration of the sensor with a flexible solid-state zinc ion battery ensures the self-powering of the sensor for various human motions detection applications.

*npj Flexible Electronics* (2022)6:92 ; https://doi.org/10.1038/s41528-022-00226-z

## INTRODUCTION

Wearable and flexible pressure sensors could be attached to the clothing or the skin to monitor external pressure, motion signals, or physiological signals under continuous working conditions[1–4]. Therefore, wearable pressure sensors are important for muscle motion analysis, sign language translation, breath monitoring, flexible electronic skins, and speech recognition applications[5–8]. There are four types of wearable sensors with different sensing mechanisms: i) piezo capacitance[3,9], ii) triboelectricity[5], iii) piezo-resistivity[10–12], and iv) piezoelectricity[13]. Among these, wearable piezoresistive pressure sensors offer advantages of low cost, easy signal collection, and low power consumption, among other interesting characteristics[12].

The application prospects of wearable piezoresistive sensors are affected by the material selection, structure design of the sensing active layer, the improvement of device performance (such as sensitivity and detection range), and the technology of reduced reliance on the external power source. Since wearable piezoresistive sensors are directly or indirectly in contact with the skin, selecting skin-friendly materials with high safety and biocompatibility as the sensing active layer is important. Hydrogels are a class of multifunctional complex polymeric materials with an obvious physically and/or chemically cross-linked 3D network structure and abundant water content[14]. Thus, hydrogels can be attached to any surface, such as our skin[14]. In general, hydrogels based on natural polymers like guar gum, sodium alginate, and chitosan show high biocompatibility, biodegradability, and good mechanical properties. These features made them useful in the fields of biomedical engineering[15], food[16], and energy storage devices[17–19], providing a breakthrough for the safety of wearable electronics. Besides, the deformation of the internal 3D skeleton of hydrogels by the external force leads to variations in the electron conduction path, which is key to improving the sensing effect. However, despite the efforts and attempts made in preparing elastic natural polymer-based hydrogels with high compressive elasticity and promoting the application of wearable pressure sensors[20,21], there are still many challenges that remain to be addressed. For instance, hydrogel-based piezoresistive sensors have unsatisfactory sensitivity. A typical way to improve sensitivity is to construct 3D microstructures on the surface of the sensing active layer by template method. Hence, numerous micro-structures, such as microwaves[22], micro-pyramids[23], microspheres[24], and micro-cylinders[25] have been explored. The number of electrical contacts can be significantly changed by the amount of applied mechanical pressure to effectively change the resistivity between the electrodes and the sensing active layer, thereby enhancing the sensitivity of the wearable piezoresistive sensors. However, the complexity of the microstructure limits the preparation under various experimental conditions. As a result, manufacturing high-sensitivity wearable piezoresistive sensors that are easy to operate remains very challenging.

Wearable piezoresistive sensors also strongly depend on the power supply. However, operating devices via external power supply in wearable technologies is difficult. Therefore, developing and combining wearable electronics with flexible energy devices for eliminating the need for an external rigid power supply is highly desirable. Accordingly, several research attempts have been made to integrate piezoresistive sensors with wearable energy storage devices[26–28]. Examples include active-powering pressure sensing fabric devices integrating zinc-air batteries with fabric-based sensing substrates[27], and all-in-one sensing patches integrated with piezo-resistive sensors and micro-supercapacitors[28]. Among various energy storage devices, solid-state zinc-ion batteries (ZIBs) are promising devices due to their environmentally friendly composition, high safety, low cost, high output voltage, and abundance of Zn[18,19]. Consequently, developing highly sensitive and wearable active-powering sensors integrated with solid-state ZIBs to continuously

[1]School of Microelectronics Science and Technology, Sun Yat-Sen University, Guangzhou, P. R. China. [2]School of Electronic and Computer Engineering, Peking University Shenzhen Graduate School, Shenzhen 518055, P. R. China. [3]School of Electronics and Information Technology, Sun Yat-Sen University, Guangzhou, P. R. China. [4]Hefei National Research Center for Physical Sciences at the Microscale, University of Science and Technology of China, Hefei 23000, P. R. China. [5]Zinergy Shenzhen Ltd., Floor 6, Building H, Gangzhilong Science Park, Longhua, Shenzhen 518109, P. R. China. [6]These authors contributed equally: Yuan Huang, Binbin Liu. ✉email: zhouh81@pkusz.edu.cn

monitor the body motions and physiological signals using simple fabrication routes is important for wearable sensors.

Herein, an elastic natural polymer-based hydrogel was constructed by utilizing locust bean gum (LBG), a natural biopolymer widely used in food, biopharmaceuticals, paper, and cosmetics[19]. The hydrogels were prepared by blending polyvinyl alcohol (PVA), LBG, and carbon nanotubes (CNTs) through a freezing method and yield a platform with a rough top surface and smooth bottom surface. The co-existence of LBG and PVA, as well as the reinforcing effect of CNTs in the polymer, led to composite hydrogels (LBG/PVA/CNTs) with superior comprehensive mechanical performances. Hydrogels with double rough surfaces (LBG/PVA/CNTs-DR) were also prepared by coupling two original hydrogels flat face to the flat face. The piezoresistive sensors composed of LBG/PVA/CNTs-DR hydrogels sandwiched between two carbon cloths exhibited a high sensitivity of 20.5 $kPa^{-1}$ under 0-1kPa, a broad detection range of 0.1–100 kPa, and good reproducibility for at least 1000 cycles. The high sensitivity of the LBG/PVA/CNTs-DR hydrogels-based piezoresistive sensor in the low-pressure range was ascribed to the huge change in the contact area between the hydrogels and the carbon cloth under loaded external pressure. Moreover, an active-powering pressure-sensing device, integrating a solid-state ZIB with the LBG/PVA/CNTs-DR hydrogels-based piezoresistive sensor into one flexible device architecture was introduced, offering a reliable, continuous body motion monitoring, and speaking signals monitoring. In sum, a low-cost and facile craft route for the fabrication of skin-friendly, high-safety, high-sensitivity, and wearable active-powering piezoresistive sensors was provided, useful for future applications.

## RESULTS AND DISCUSSION

### Fabrication and characterization of LBG/PVA/CNTs hydrogels

In this work, PVA, LBG, and CNTs were employed to fabricate composite hydrogels by freezing method, followed by peeling off from the gel mold (Fig. 1a). The hydrogels benefited from the distinctive individual and complementing characteristics of PVA, CNTs, and LBG. The high mechanical strength and elasticity of PVA made it a useful primary polymer network. The LBG and PVA molecules containing large numbers of hydrogen bonds directly formed intra- and inter-hydrogen bonds (Fig. 1b). The hydrogen bonds between LBG and PVA further enhanced the mechanical strength of the network structure. CNTs were essential for constructing a conductive 3D network. The surface morphologies of the top surface and bottom surface of the hydrogels were observed by scanning electron microscopy (SEM) and the results are shown in Fig. 1c. The top surface of the LBG/PVA/CNTs hydrogels revealed an irregular scaly-shaped structure, naturally generated during hydrogel formation. By contrast, the bottom surface of the LBG/PVA/CNTs hydrogels displayed a smooth and flat structure, templated from a smooth surface of the petri dish (Fig. 1d). The surface roughness of the top and bottom surface of LBG/PVA/CNTs hydrogels was further evaluated by laser scanning confocal microscopy (Fig. 1e, f). The 2D view proved the top surface to possess a larger surface undulation range (0-421 μm) and average roughness (Ra = 45.6 μm) when compared to the bottom surface (0–200 μm, Ra = 9.2 μm). Figure 1g shows the roughness of the top and bottom surfaces of the LBG/PVA/CNTs hydrogels is reproducible. As shown in Fig. 1g, the average roughness of the top surfaces is (45.6 μm, 44.2 μm, 50.1 μm) of three hydrogels sample are much higher than that of the bottom surfaces (9.2 μm, 4.8 μm, 8.3 μm). The mean and variance of roughness of the top surfaces is 46.63 μm and 6.34 μm, respectively. The mean and variance of roughness of the bottom surfaces is 7.43 μm and 3.60 μm, respectively. Moreover, the roughness of the top surface of hydrogels is tunable by adjusting the LBG/PVA mass ratio and the freezing temperature. For example, the top surface of the LBG/PVA/CNTs hydrogels with LBG/PVA mass ratio of 1:2, 1:4 and 1:8 possess average roughness of 18.4, 45.6 and 20.0 μm, indicating the roughest top surface of the hydrogel with an LBG/PVA mass ratio of 1:4, as shown in Fig. 1h. We further test the roughness of the top surface of LBG/PVA/CNTs hydrogels with various freezing temperature (−10 °C, −20 °C, −30 °C). The top surface of hydrogels with various freezing temperature (−10 °C, −20 °C, −30 °C) possess average roughness of 35.5, 45.6 and 29.1 μm, as shown in Supplementary Fig. 1. Based on these experiments, it is found both LBG/PVA mixing ratio and the freezing temperature can affect the top surface roughness of the blended gel, while the former has higher impact than the latter.

In order to evaluate the effect of LBG on the mechanical performance of the hydrogels, the tensile and compressive tests were performed for quantitative comparison of mechanical performance of LBG/PVA/CNTs and PVA/CNTs hydrogels. As shown in Supplementary Fig. 2a, the tensile strength of LBG-PVA-CNTs increased to 0.3 MPa, while the fracture elongation rose to 438%. By comparison, the PVA/CNTs hydrogel presented a relatively low tensile strength of 0.08 MPa and large fracture elongation of 266%. In addition, the compressive properties were also highly promoted, as shown in Supplementary Fig. 2b. At compressive strain of 80%, the compressive stress of LBG/PVA/CNTs hydrogel reached as high as 0.12 MPa, a value of 1.7-fold higher than that of PVA/CNTs hydrogels (0.07 MPa). Thus, the introduction of LBG enhanced the mechanical strength of the LBG/PVA/CNTs hydrogels, arising from the hydrogen bonds between LBG and PVA. We also investigated the effect of different LBG/PVA mass ratio on the compressive properties of the hydrogels. The results in Supplementary Fig. 3 show that the LBG/PVA/CNTs hydrogel with an LBG/PVA mass ratio of 1:4 exhibits the best compressive properties among these samples.

The co-existence of LBG and PVA, as well as the reinforcing effect of CNTs in the polymer matrices induced LBG/PVA/CNTs hydrogels with superior comprehensive mechanical performances. In Supplementary Fig. 2c, the LBG/PVA/CNTs hydrogels were twisted arbitrarily. The LBG/PVA/CNTs hydrogels also stretched more than three times the initial length without breaking (Supplementary Fig. 2d). In addition to high stretchability, the hydrogels could bear up to 200 g weight without breaking, demonstrating LBG/PVA/CNTs hydrogels with good mechanical strength (Supplementary Fig. 2e). Furthermore, the hydrogels demonstrated superb compressive elasticity that can be compressed without breaking and recover to the original shape after releasing the compressive force (Supplementary Fig. 2f). Overall, the LBG/PVA/CNTs hydrogels were suitable as sensing active layers for flexible piezoresistive sensors.

### Sensing performance of the sensors

To characterize and optimize the performances of the devices, the piezoresistive sensors with the LBG/PVA/CNTs hydrogels sandwiched between two carbon cloth electrodes were fabricated. Sensitivity ($S$) is an important parameter for evaluating the performance of sensors, which can be calculated by the formula:

$$S = \delta((I - I_0)/I_0)/\delta P,$$

where $I_0$ and $I$ are the initial currents without pressure loading and the responsive current under loading, respectively, and $P$ is the value of pressure. Accordingly, low $I_0$ and high $I$ would be beneficial for achieving high sensitivity for piezoresistive sensors.

To achieve a low $I_0$, hydrogels with double rough surfaces were prepared by coupling two pieces of original hydrogels flat face to flat face (Fig. 2a). This fashion would reduce the initial contact area between the hydrogels and carbon cloth electrode. The optical microscopy images in Supplementary Fig. 4 showed changes in

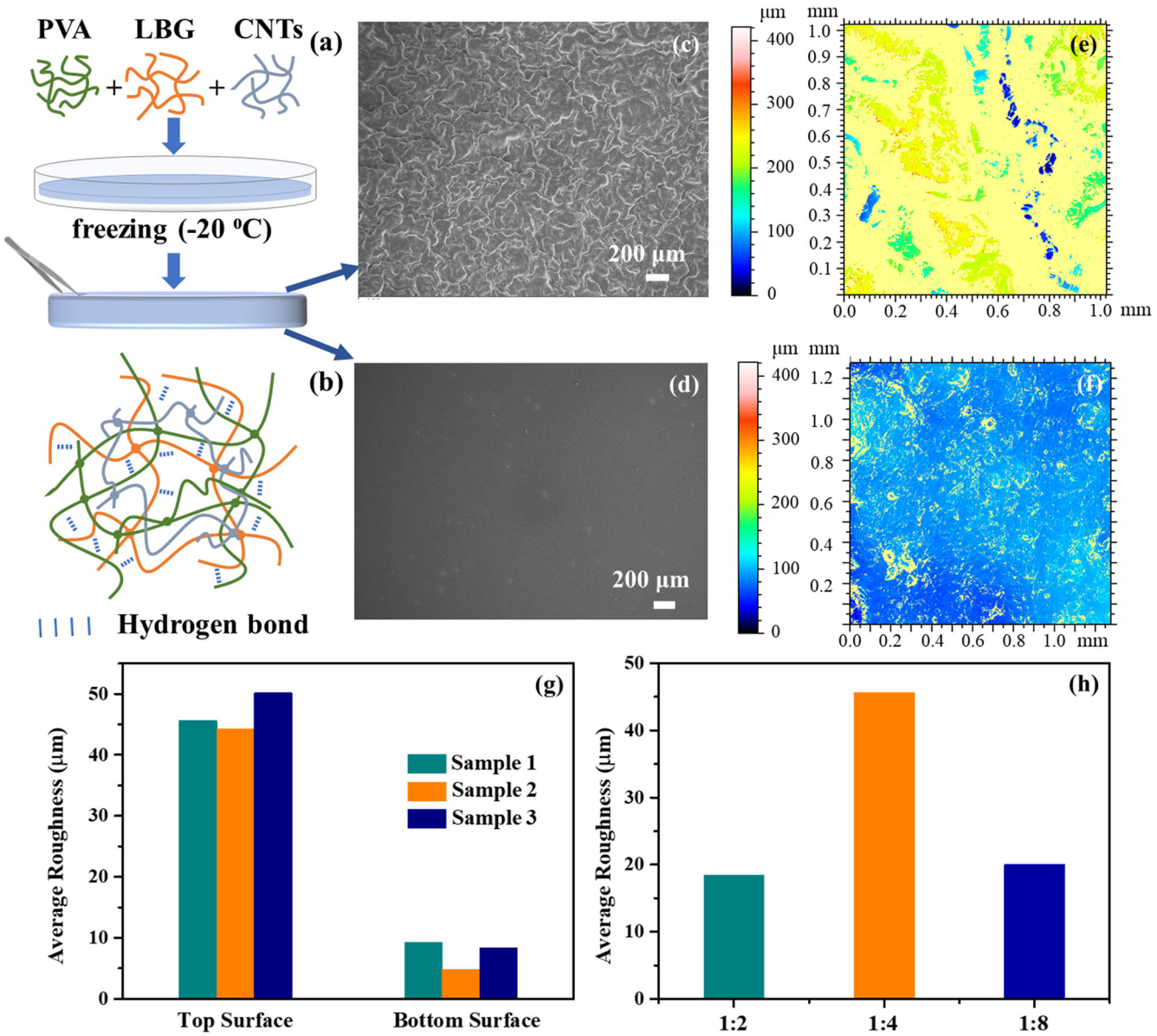


**Fig. 1 Fabrication steps and morphology characterization. a** Schematic illustration of the fabrication of LBG/PVA/CNTs hydrogel. **b** Illustration of the LBG/PVA/CNTs hydrogel. SEM images of **c** the top surface and **d** the bottom surface of LBG/PVA/CNTs hydrogels. 2D profiles of **e** the top surface and **f** the bottom surface of LBG/PVA/CNTs hydrogels measured by a laser scanning confocal microscope. **g** The average roughness of the top and bottom surface for LBG/PVA/CNTs hydrogels. **h** The average roughness of the top surface for LBG/PVA/CNTs hydrogels with LBG/PVA mass ratio of 1:2, 1:4 and 1:8.

the gap between the two pieces of LBG/PVA/CNTs hydrogel after coupling. After 48 h, no obvious gap was noticed between the flat surfaces of the two pieces of the hydrogel. For comparison, the hydrogels with double flat surfaces by coupling two pieces of original hydrogels rough face to rough face (Fig. 2b), as well as the original LBG/PVA/CNTs hydrogels with a single rough surface (Fig. 2c) also acted as sensing active layers for piezoresistive sensors. Note that the LBG/PVA/CNTs hydrogels with double rough surfaces, double flat surfaces, a single rough surface and were denoted as LBG/PVA/CNTs-DR, LBG/PVA/CNTs-DF, LBG/PVA/CNTs-SR hydrogels, respectively.

The influences of surface morphologies of hydrogels on the performances of the resulting sensors were investigated. In Fig. 2d, by plotting each applied pressure and current response point by point, the change in the ratio of current as a function of applied pressure was obtained. The sensor with LBG/PVA/CNTs-DR hydrogel revealed the highest sensitivity among all the sensors. According to the linear fitting results, the sensitivities of the sensor with LBG/PVA/CNTs-DR hydrogels can be divided into three regions: low-pressure range (0.1–1 kPa, 20.5 $kPa^{-1}$), medium-pressure range (1–10 kPa, 2.28 $kPa^{-1}$), and high-pressure range (10–100 kPa, 0.24 $kPa^{-1}$). However, though the sensor with LBG/PVA/CNTs-SR hydrogels showed a good piezoresistive sensing response (0.4–4 kPa, 2.41 $kPa^{-1}$; 4-10 kPa, 0.85 $kPa^{-1}$; 10–100 kPa, 0.14 $kPa^{-1}$), its sensitivities were less than those of sensor with LBG/PVA/CNTs-DR hydrogels. According to the calculations, the sensitivities of the sensor with LBG/PVA/CNTs-DR hydrogels were 8.5-fold (0.4–1 kPa), 2.7-fold (4–10 kPa) and 1.7-fold (10–100 kPa) higher than those of the sensor with LBG/PVA/CNTs-SR hydrogels, respectively. The sensor with LBG/PVA/CNTs-DF hydrogels showed the worst piezoresistive sensing response (0.4–20 kPa, 0.0272 $kPa^{-1}$; 20-50 kPa, 0.0176 $kPa^{-1}$; 50-100 kPa, 0.0084 $kPa^{-1}$). Therefore, the sensor-based on LBG/PVA/CNTs-DR hydrogel with a good linear range (0.1–100 kPa)

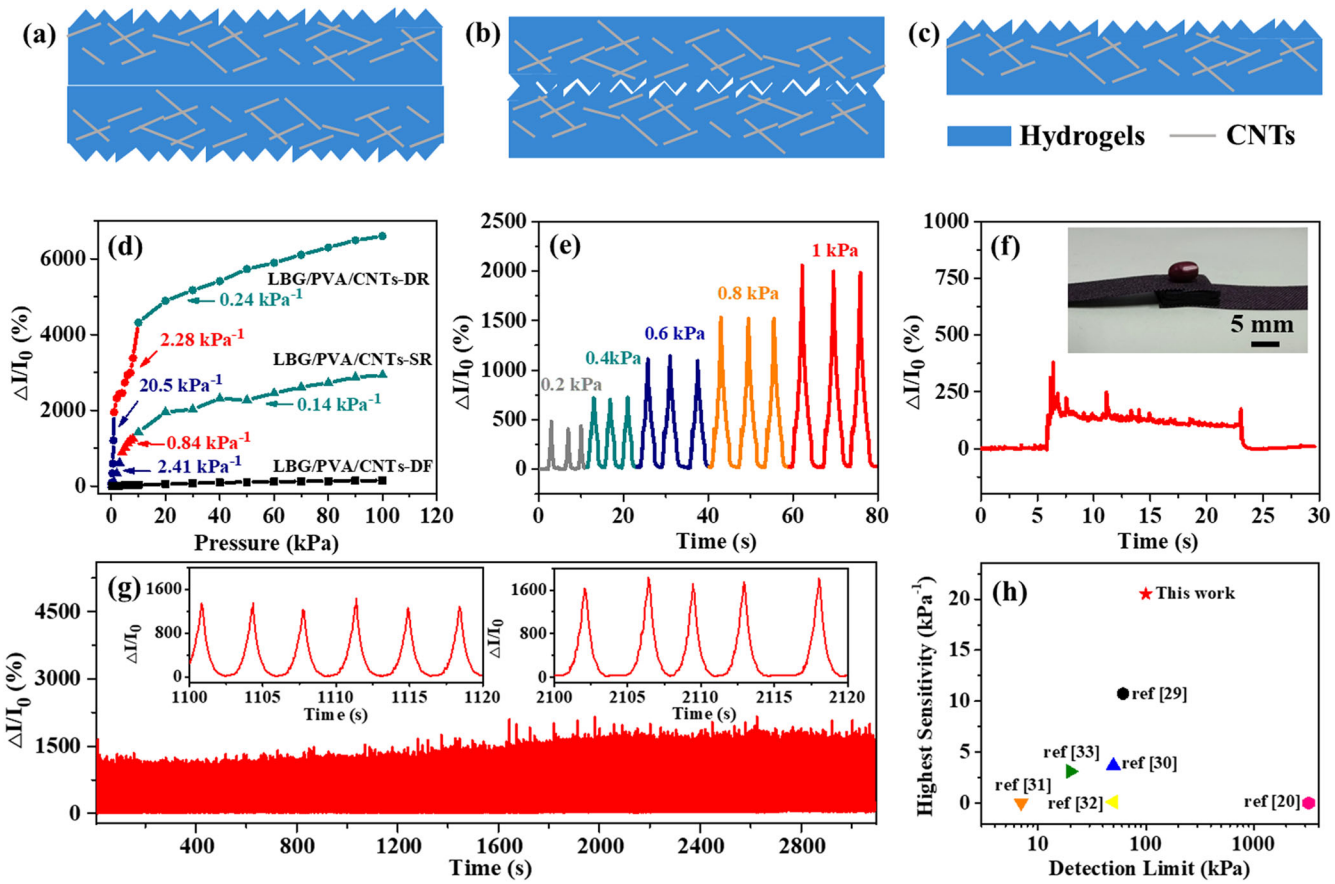


**Fig. 2 Evaluation of the performance of the sensor.** Schematic illustration of **a** LBG/PVA/CNTs-DR, **b** LBG/PVA/CNTs-DF and **c** LBG/PVA/CNTs-SR hydrogels. **d** The relative current changes for the sensors with LBG/PVA/CNTs-SR, LBG/PVA/CNTs-DF and LBG/PVA/CNTs-DR hydrogels; the slope of the curve represents sensitivity. **e** The I-t curves of the sensor with LBG/PVA/CNTs-DR hydrogels under serial pressures below 1 kPa. **f** Response of the sensor with LBG/PVA/CNTs-DR hydrogels to the loading and removal of a small weight (a grain of beans, corresponding to a pressure below 0.1 kPa). **g** Durability test of the sensor with LBG/PVA/CNTs-DR hydrogels for 1000 cycles under 0.8 kPa. **h** Detection limit and sensitivity of our piezoresistive sensor with LBG/PVA/CNTs-DR hydrogels in comparison with piezoresistive sensors based on hydrogels as reported in refs. [20,29–33].

and high sensitivity (20.5 $kPa^{-1}$ under 0–1 kPa) was selected for subsequent experiments.

To verify the reliability of the sensor with LBG/PVA/CNTs-DR hydrogels, different dynamic pressures were applied to the sensor. As shown in Fig. 2e, the increase in applied pressure led to raised current response simultaneously. Hence, the LBG/PVA/CNTs-DR hydrogels-based sensors can accurately distinguish between different levels of force even in the low-pressure range. Moreover, the device detected tiny pressures below 0.1 kPa (Fig. 2f, mass of the bean 0.1 g). The relative current fluctuation during the measurement in Fig. 2f originates from the metastable contact between the sensor and the bean.

The long-term stability of the sensor was also studied and the data are gathered in Fig. 2g. The LBG/PVA/CNTs-DR hydrogels-based sensor was tested for 1000 cycles of continuous operation under 0.8 kPa. As can be seen, the relative current changes did not demonstrate any degradation, indicating the good stability of the prepared device. It is worth noting that the relative current change increases during the durability test. The test is measured at room temperature. As the hydrogels exhibited low rate for weight loss at room temperature (Supplementary Fig. 5), the increase in the relative current change is not caused by enhanced conductivity due to shrinkage from evaporation. The increase in the relative current change is then deduced to be associated with the air gap between layers of LBG/PVA/CNTs composite hydrogel. The air gap disappears after multiple cycles pressure test and the contact area between two layers of LBG/PVA/CNTs composite hydrogel increases.

Compared to other reported sensors with hydrogels as active sensing layers[20,29–33], the proposed sensor with LBG/PVA/CNTs-DR hydrogel was advantageous in terms of sensitivity and linear detection range (Fig. 2h and Supplementary Table 1). The good performances would have potential prospects in many application fields, such as wearable electronic products and human-computer interaction interface systems.

## The sensing mechanism of the sensor with LBG/PVA/CNTs-DR hydrogels

The sensor with LBG/PVA/CNTs-DR hydrogels showed a high sensitivity (20.5 $kPa^{-1}$) in detecting small pressures (0–1kPa) with a wide detection range (0–100 kPa), clearly demonstrating outstanding piezoresistive sensing performance. An overall structural schematic diagram of the sensor composed of the LBG/PVA/CNTs-DR hydrogel sandwiched between two carbon cloth electrodes is provided in Fig. 3a. The changing processes of the contact points between carbon cloth and hydrogels, as well as the deformation of carbon cloth and LBG/PVA/CNTs-DR hydrogels under the action of external force, are presented in Fig. 3b–d. Initially in the absence of applied pressure, the contact points between carbon cloth and the rough hydrogels were few to create an electric current conduction path, leading to a low $I_0$. Note that the low initial $I_0$ created a low noise level, critical for achieving high sensitivity.

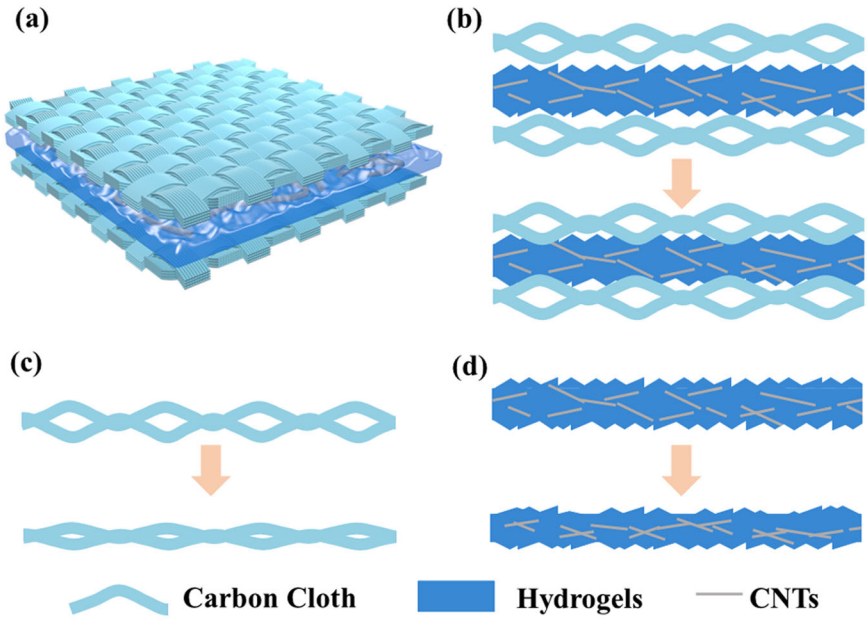


**Fig. 3 Schematic description of sensing mechanism. a** Schematic diagram of the structure of the sensor with LBG/PVA/CNTs-DR hydrogels and (**b**–**d**) its mechanism analysis of the pressing process.

Upon the application of tiny external pressure (0–1 kPa) to the sensor (Fig. 3b), the contact area between carbon cloth and hydrogels increased. This changed the output electrical signal significantly, resulting in a high sensitivity of 20.5 $kPa^{-1}$ in the low-pressure detecting range (0–1 kPa). As pressure increased to a medium range (1–10 kPa), the effective contact area between carbon cloth and hydrogels gradually reached saturation, while the compression of carbon fiber in carbon cloth just started to occur (Fig. 3c). At this stage, the decreasing rate in the total resistance of the sensor slowed down, and the sensitivity decreased to 2.28 $kPa^{-1}$ (1–10 kPa). Further increase in pressure (10–100 kPa) initiated the deformation of the CNT network inside LBG/PVA/CNTs-DR hydrogels (Fig. 3d), thereby reducing the resistance of the hydrogels. At this stage, the sensor only showed a lower sensitivity of 0.24 $kPa^{-1}$ in the pressure range of 10–100 kPa. The multiple responsiveness of the sensor was beneficial to obtain high sensitivity and wide detection range, but not conducive to obtaining a fast response time. In this work, the sensor exhibited a response time of 356 ms and a recovery time of 355 ms (Supplementary Fig. 6), limited by the multiple responsiveness of the sensor[11].

## Parameter optimization of the sensor

The results also revealed the important role of the double rough surface of LBG/PVA/CNTs-DR hydrogels in the sensor. The double rough surface would facilitate the formation of a huge contact interface between hydrogels and carbon cloth electrode, so that the electron flow path would increase instantaneously when the electrode was in contact with the rough surface of the hydrogels under small applied external force, resulting in a sharp drop in contact resistance. This helped increase the sensitivity of the sensor, explaining the higher sensitivity of the sensor based on LBG/PVA/CNTs-DR hydrogel when compared to the sensors based on LBG/PVA/CNTs-SR hydrogel or LBG/PVA/CNTs-DF hydrogel.

Features like the amount of CNTs in the hydrogels, the morphology, and the conductivity of the electrode also affected the performance of the sensor. As shown in Supplementary Fig. 7, the sensitivity of the sensor prepared with LBG/PVA/CNTs-DR hydrogel depended on the amount of CNTs in the hydrogels. Insufficient amounts of CNTs did not fill the hydrogels uniformly, whereas excess amounts of CNTs increased the $I_0$ without pressure loading. Experimentally, the optimal CNTs/LBG ratio was identified as 3:10 in experiments. Besides the amount of CNTs in the hydrogels, the sensitivity of the sensor with LBG/PVA/CNTs-DR hydrogel depended on the nature of the electrode substrate. Supplementary Fig. 8 compares the response of the sensor based on the Cu electrode and carbon cloth. Clearly, the sensor prepared with carbon cloth achieved lower $I_0$ ($10^{-7}$ A vs $10^{-4}$ A) and a higher response than that prepared with a Cu electrode. On the one hand, the Cu electrode with a better conductivity ($3.4 \times 10^{-4}$ Ω/sq vs 0.6 Ω/sq) did not look as sensitive to pressure as carbon cloth since its conductivity was higher in a pressure-free state. In other words, the difference between the stress-free state and the pressure-saturated state was smaller. On the other hand, the surface of the carbon cloth looked much rougher (Supplementary Fig. 10a, b), forming a lower initial contact area between the hydrogels and the electrode to enhance the sensing performance. Therefore, the carbon cloth with moderate conductivity and a rough surface was another critical component for achieving high-performance pressure sensors.

## Applications of the sensor

The above results and analyses indicated that the sensor with LBG/PVA/CNTs-DR hydrogel exhibited good sensing performance. The sensor was further used as a switch in series with the light emitting diode (LED) connected to a 5 V direct current power supply to turn on/off the LED (Fig. 4a). The LED was off in the original state and it was on when the sensor was compressed.

The high-performance sensor was also used to accurately detect human motion signals. To this end, we attached our sensor to the fingers and wrists to monitor movements. As shown in Fig. 4b, c, the sensor can be used to detect the pressure produced by finger bending (50°, 65°, and 90°, Fig. 4b) and the signal waveform of wrist bending remains consistent under the same bending angle (60°, Fig. 4c). By attaching the sensor onto the throat, speaking signals of the word ni hao (Fig. 4d), sensor (Fig. 4e), and chuan gan qi (Fig. 4f) were also recognized separately. Thus, the sensor possessed significant potential applications in indiscriminating different types of deformation and speech recognition.

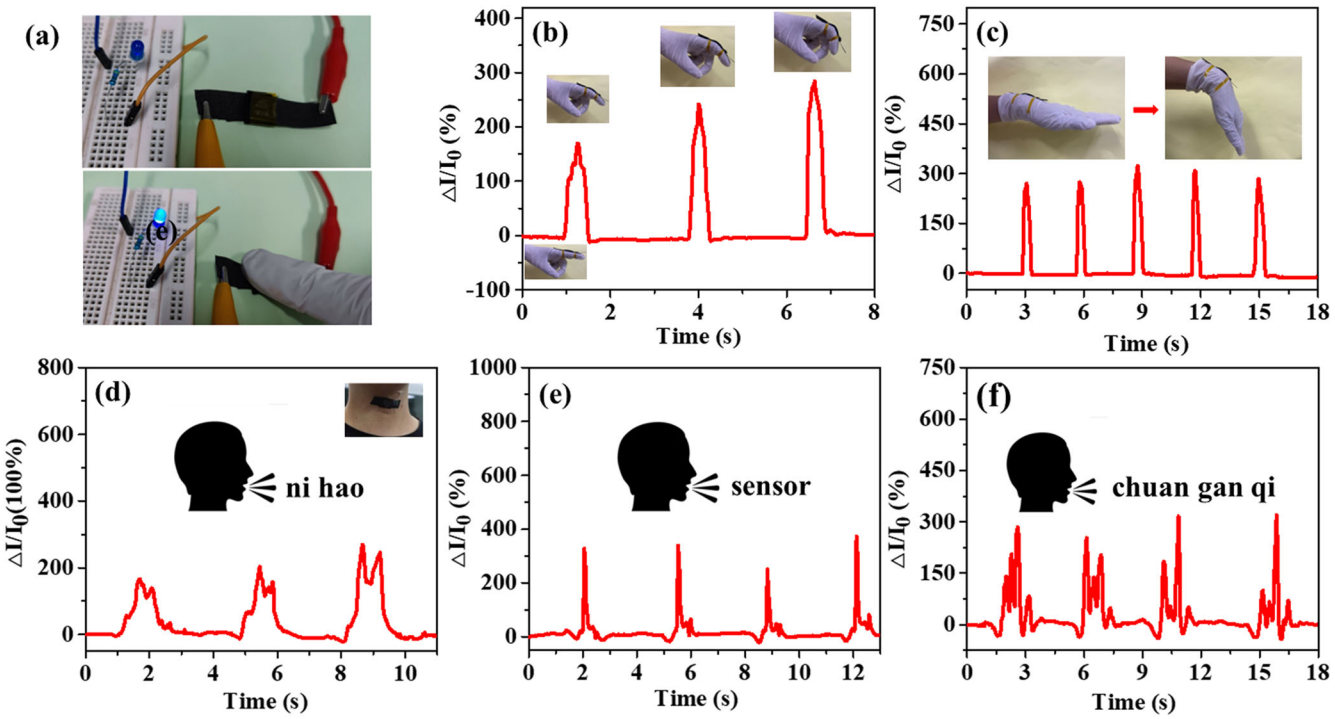


**Fig. 4 Applications of the sensor for various signal detection. a** The sensor used as a switch in series with the LED and the power supply to turn on/off LED. The signal responses arise from (**b**) finger bending, (**c**) wrist bending, and speaking (**d**) ni hao, (**e**) sensor, (**f**) chuan gan qi.

### The monolithic integration of the sensor and flexible ZIB

To test the potential of the proposed devices as wearable electronics without the need for an external rigid power supply, the sensor prepared with LBG/PVA/CNTs-DR hydrogel was further monolithically integrated with a flexible solid-state ZIB based on LBG hydrogel electrolyte. As illustrated in Fig. 5a, such an active-powering pressure-sensing device had two stacking functional structures. The solid-state ZIB sitting on top of the sensor with LBG/PVA/CNTs-DR hydrogel consisted of five distinct layers, of which three layers were made from commercially available carbon cloth, and the other two layers were hydrogels based on natural polymer. From the top to the bottom, the flexible ZIB was made of three flexible layers: a $MnO_2$ cathode, an LBG hydrogel electrolyte, and the electro-deposited Zn anode on carbon cloth. Moreover, the ZIB and the pressure sensors shared a common carbon cloth electrode sandwiched in the middle of the stacks. Consecutively, the piezoresistive sensor was made up of another three-layer stacking structure with the top electrode shared between flexible ZIB, LBG/PVA/CNTs-DR hydrogel as an active sensing layer, and a bottom electrode layer of carbon cloth. The charge-discharge characteristics of the ZIB are reported in our previous work[19]. The discharge voltage plateau is ~1.4 V. To verify the distinct self-powering feature, the wearable device was connected to a homemade signal management circuit system (Fig. 5b, c). The key electronic components employed in the signal management circuit system include a micro-controller unit (MCU) (STM32L051C8T6, STMicroelectronics), a Bluetooth low energy (BLE) module (BT691, Feasycom), a voltage boosting boost chip (TLV61220, TI), an analog-to-digital converter (ADC, which is integrated in the MCU), and a sampling resistor.

The entire circuit is simplified by the circuit diagram in Fig. 5c. A commercial voltage boosting chip is used to raise the voltage of the ZIB to 2 V, which is sufficient to power the MCU and the BLE. Upon application of pressure, the resistance of the wearable sensor changed, resulting in the variation of voltage across the sampling resistor. Here, a dual-channel ADC was used to measure the voltage across the sensor and the voltage of the battery simultaneously. Thus, the accurate voltage drop on the sampling resistor can be obtained by subtracting the voltage drop on the sensor from the voltage of the battery, and finally the current flowing through the sensor can be attained without being affected by the voltage drop in the battery. On the other hand, the voltage drop on the sensor is directly measured by the ADC. As a result, the effect of the voltage drop in the battery can be corrected. The recorded digital signal was then transmitted to a mobile device by BLE. Both the MCU and the BLE are set to the low-power mode. The total operation current of the MCU and the BLE drawn from the ZIB is about 2.2 mA, and the overall power consumption of the signal management circuit system is calculated to be only 3.1 mW. Therefore, the capacity of the ZIB (2.72 mAh) is capable of powering an MCU with BLE continuously for 1.2 hours.

Using the circuitry shown in Fig. 5c, the real-time pronunciation monitoring measurement signal can wirelessly be transmitted by a Bluetooth device and displayed on a computer via a custom interface (Fig. 5d, e). The waveforms of pressing signal and speaking signals of the word hello collected from the wireless data transmission sensor system are plotted in Fig. 5f and Fig. 5g. Important features of the waveforms were observed, showing a sensing system with great potential for use in on-line monitoring and intelligent speech recognition with advantages of being compact, lightweight, and wireless, without the need of rigid external power supply.

In summary, a simple and efficient method was developed to fabricate a conductive, elastic, and biocompatible hybrid network hydrogel by cross-linking LBG, PVA, and CNTs. The resulting LBG/PVA/CNTs hydrogel with a double rough surface could be prepared by coupling two original hydrogels flat face to the flat face. A piezoresistive sensor was assembled with the as-obtained hydrogel sandwiched between two carbon cloth electrodes. The huge change in the contact area between the hydrogels and the carbon cloth resulted in a piezoresistive sensor with a high sensitivity of 20.5 $kPa^{-1}$ under 0-1kPa, a broad detection range of 0.1–100 kPa, and good reproducibility for at least 1000 cycles. Moreover, when integrating with a solid-state ZIB, the sensor functioned in a self-powered manner to detect various human motions. In sum, these

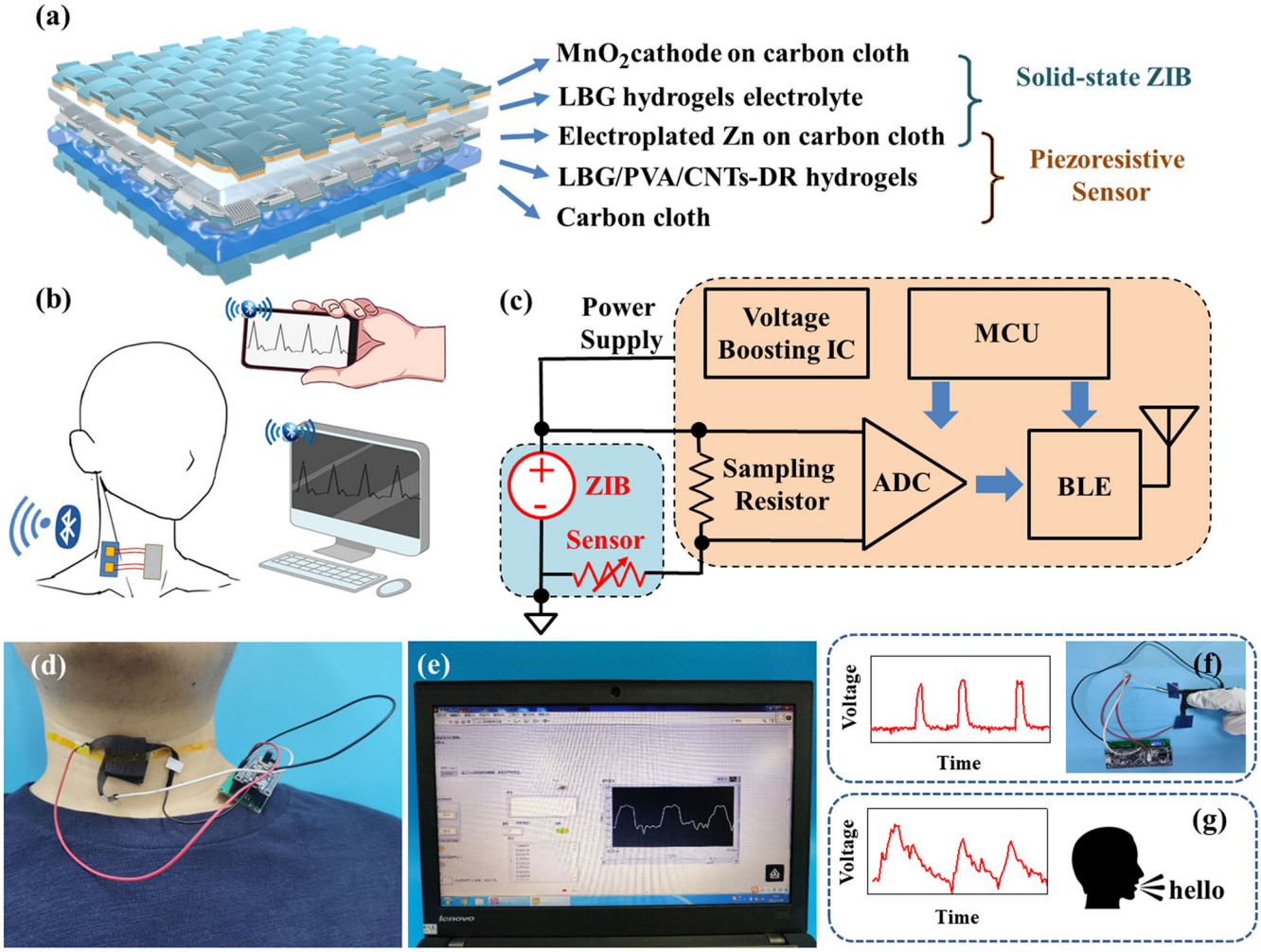


**Fig. 5 The monolithic integration of the sensor with LBG/PVA/CNTs-DR hydrogel and flexible ZIB. a** Schematic illustrations of the active powering senser integrated with a solid-state ZIB in the layer-by-layer view. **b** Schematic illustrations of the active powering senser with a solid-state ZIB and a signal management circuit system mounted on the throat to monitor pronunciation. **c** A simplified circuit diagram of the active powering senser with a solid-state ZIB and a homemade signal management circuit system. **d** Photograph of the active powering senser with a solid-state ZIB and a homemade signal management circuit system mounted on the throat to monitor pronunciation. **e** Photograph showing that the real-time pronunciation monitoring measurement signal can be wireless transmitted by a Bluetooth device and displayed on a computer via a custom interface. Detection of the real-time pulse signals from (**f**) pressing and (**g**) speaking signals of the word hello.

findings look promising for the preparation of green and high-performance piezoresistive sensors.

## METHODS

### Preparation of LBG/PVA/CNTs hydrogel

LBG/PVA/CNTs hydrogel was prepared in three steps. First, 4 g polyvinyl alcohol (PVA, 1750 ± 50, Shanghai yuanye Bio-Technology Co., Ltd.) and 300 mg Carbon Nanotube (CNT, XFM17, Nanjing/Jiangsu XFNANO Materials Tech Co., Ltd.) were added to 40 mL water and heated to 100 °C under vigorous stirring until all PVA was fully dissolved. Second, 1 g locust bean gum (LBG, Aladdin) and the above solution were mixed by stirring until homogeneous dissolution. The resulting mixture was then poured into a petri dish and transferred to an environmental cabinet at −20 °C for 12 h. The PVA/CNTs hydrogels were prepared by a similar method without the introduction of LBG.

### Preparation of ZIB

The ZIB was assembled with LBG electrolyte, $MnO_2$/reduced graphene oxide ($MnO_2$/rGO) cathode and the electro-deposited Zn anode[19]. A $MnO_2$/rGO cathode (70 wt% of α-$MnO_2$ (obtained by the hydrothermal method), 20 wt% of rGO (Nanjing/Jiangsu XFNANO Materials Tech Co., Ltd.), and 10 wt% of polyvinylidene fluoride (PVDF)) on carbon cloth was prepared. The Zn anode was obtained by electrodeposition of Zn on carbon cloth[19]. The LBG electrolyte was prepared by dispersing 0.5 g LBG in 10 mL aqueous solution containing 2 M $ZnSO_4$ (AR grade, Aladdin) and 0.1 M $MnSO_4$ (AR grade, Macklin) at room temperature, followed by a heating process at 100 °C for 5 min[19].

### Characterization

The surface morphologies of the hydrogels were examined by field-emission scanning electron microscopy (FESEM, Zeiss SUPRA-55). A 3D laser scanning confocal microscope (LSCM-Zeiss-LSM900) was used for the analysis of the surface roughness of the LBG/PVA/CNTs hydrogel.

The tensile and compressive mechanical properties of LBG/PVA/CNTs hydrogel and PVA/CNTs hydrogel were tested by ESM 303 equipped with a force gauge model M5-5 (maximum force: 25 N), Mark-10. The tensile tests were conducted on a rectangular sample (25*10*1.5 $mm^3$) at 20 mm $min^{-1}$. The compressive tests were

conducted on a cylindrical sample (diameter: 10 mm, height: 1.5 mm) at 20 mm $min^{-1}$.

The LBG/PVA/CNTs-DR hydrogels with double rough surfaces were prepared by coupling two original hydrogels flat face to flat face. For comparison, the original LBG/PVA/CNTs hydrogels with single rough surface (LBG/PVA/CNTs-SR) and hydrogels with double flat surfaces (LBG/PVA/CNTs-DF) were obtained by coupling two original hydrogels rough face to rough face. The hydrogels were tailored into 1 cm × 1 cm square pieces. The piezoresistive sensor was assembled by employing the hydrogels as the sensing active layer and carbon cloth as electrodes. For the device characterization, the I-t data were collected by a digital source meter (Keithley 2602B) at the working voltage of 1.5 V.

## DATA AVAILABILITY

The data that support the findings of this study are available from the corresponding author upon reasonable request.

Received: 27 July 2022; Accepted: 1 November 2022;
Published online: 10 November 2022

## REFERENCES

1. Gao, F. et al. A stretching-insensitive, self-powered and wearable pressure sensor. *Nano Energy* **91**, 106695 (2022).
2. Weng, X., Zhang, C., Feng, C. & Jiang, H. Facile fabrication of an ultrasensitive all-fabric wearable pressure sensor based on phosphorene-cold nanocomposites. *Adv. Mater. Interfaces* **9**, 2102588 (2022).
3. Ha, K. H. et al. Highly sensitive capacitive pressure sensors over a wide pressure range enabled by the hybrid responses of a highly porous nanocomposite. *Adv. Mater.* **33**, 2103320 (2021).
4. Cui, X. et al. Flexible and breathable all-nanofiber iontronic pressure sensors with ultraviolet shielding and antibacterial performances for wearable electronics. *Nano Energy* **95**, 107022 (2022).
5. Li, J. et al. Biologically inspired stretchable, multifunctional, and 3D electronic Skin by strain visualization and triboelectric pressure sensing. *Small Sci.* **2**, 2100083 (2022).
6. Meng, K. et al. Wearable pressure sensors for pulse wave monitoring. *Adv. Mater.* **34**, 2109357 (2022).
7. Jeong, Y. et al. Ultra-wide range pressure sensor based on a microstructured conductive nanocomposite for wearable workout monitoring. *Adv. Healthc. Mater.* **10**, 2001461 (2021).
8. Zou, X. et al. Ultrahigh sensitive wearable pressure sensors based on reduced graphene oxide/polypyrrole foam for sign language translation. *Adv. Mater. Technol.* **6**, 2001188 (2021).
9. Guan, F. et al. Silver nanowire–bacterial cellulose composite fiber-based sensor for highly sensitive detection of pressure and proximity. *ACS Nano* **14**, 15428–15439 (2020).
10. Li, L., Bao, X., Meng, J., Zhang, C. & Liu, T. Sponge-hosting polyaniline array microstructures for piezoresistive sensors with a wide detection range and high sensitivity. *ACS Appl. Mater. Interfaces* **14**, 30228–30235 (2022).
11. Xu, M. et al. Breathable, degradable piezoresistive skin sensor based on a sandwich structure for high-performance pressure detection. *Adv. Electron. Mater.* **7**, 2100368 (2021).
12. Wang, X. et al. Sea urchin-like microstructure pressure sensors with an ultra-broad range and high sensitivity. *Nat. Commun.* **12**, 1776 (2021).
13. Lu, J. et al. A Biodegradable and recyclable piezoelectric sensor based on a molecular ferroelectric embedded in a bacterial cellulose hydrogel. *ACS Nano* **16**, 3744–3755 (2022).
14. Zhao, W., Zhang, D., Yang, Y., Du, C. & Zhang, B. A fast self-healing multifunctional polyvinyl alcohol nano-organic composite hydrogel as a building block for highly sensitive strain/pressure sensors. *J. Mater. Chem. A* **9**, 22082–22094 (2021).
15. Gaharwar, A. K., Peppas, N. A. & Khademhosseini, A. Nanocomposite hydrogels for biomedical applications. *Biotechnol. Bioeng.* **111**, 441–453 (2014).
16. Klein, M. & Poverenov, E. Natural biopolymer-based hydrogels for use in food and agriculture. *J. Sci. Food Agr.* **100**, 2337–2347 (2020).
17. Ji, D. et al. Superstrong, superstiff, and conductive alginate hydrogels. *Nat. Commun.* **13**, 3019 (2022).
18. Wang, J. et al. Flexible and anti-freezing zinc-ion batteries using a guar-gum/sodium-alginate/ethylene-glycol hydrogel electrolyte. *Energy Storage Mater.* **41**, 599–605 (2021).
19. Liu, B. et al. Highly conductive locust bean gum bio-electrolyte for superior long-life quasi-solid-state zinc-ion batteries. *RSC Adv.* **11**, 24862–2487 (2021).
20. Yang, Y. et al. Anti-freezing, resilient and tough hydrogels for sensitive and large-range strain and pressure sensors. *Chem. Eng. J.* **403**, 126431 (2021).
21. Shen, X. et al. Double-network hierarchical-porous piezoresistive nanocomposite hydrogel sensors based on compressive cellulosic hydrogels deposited with silver nanoparticles. ACS Sustain. *Chem. Eng.* **8**, 7480–7488 (2020).
22. Park, J., Kim, M., Lee, Y., Lee, H. S. & Ko, H. Fingertip skin–inspired microstructured ferroelectric skins discriminate static/dynamic pressure and temperature stimuli. *Sci. Adv.* **1**, 1500661 (2015).
23. Sun, F. et al. Novel flexible pressure sensor combining with dynamic-time-warping algorithm for handwriting identification. *Sens. Actuators A* **293**, 70 (2019).
24. Zhang, Y. et al. Flexible and highly sensitive pressure sensors with surface discrete microdomes made from self-assembled polymer microspheres array. *Macromol. Chem. Phys.* **221**, 2000073 (2020).
25. Peng, S., Blanloeuil, P., Wu, S. & Wang, C. H. Rational design of ultrasensitive pressure sensors by tailoring microscopic features. *Adv. Mater. Interfaces* **5**, 1800403 (2018).
26. Li, Y., Guan, Q., Cheng, J. & Wang, B. Amorphous H0.82 MoO3.26 cathodes based long cyclelife fiber-shaped Zn-ion battery for wearable sensors. *Energy Storage Mater.* **49**, 227–235 (2022).
27. Sun, H. et al. Active-powering pressure-sensing fabric devices. *J. Mater. Chem. A* **8**, 358–368 (2020).
28. Song, Y. et al. All-in-one piezoresistive-sensing patch integrated with micro-supercapacitor. *Nano Energy* **53**, 189–197 (2018).
29. Lu, Y. et al. Highly stretchable, elastic, and sensitive MXene-based hydrogel for flexible strain and pressure sensors. *Research* **1**, 2038560 (2020).
30. Yin, M., Zhang, Y., Yin, Z., Zheng, Q. & Zhang, A. P. Micropatterned elastic gold-nanowire/polyacrylamide composite hydrogels for wearable pressure sensors. *Adv. Mater. Technol.* **3**, 1800051 (2018).
31. Ge, G. et al. Stretchable, transparent, and self-patterned hydrogel-based pressure sensor for human motions detection. *Adv. Funct. Mater.* **28**, 1802576 (2018).
32. Qin, Z. et al. Carbon nanotubes/hydrophobically associated hydrogels as ultra-stretchable, highly sensitive, stable strain, and pressure sensors. *ACS Appl. Mater. Interfaces* **12**, 4944–4953 (2020).
33. Gao, Y. et al. Flexible and sensitive piezoresistive electronic skin based on TOCN/PPy hydrogel films. *J. Appl Polym. Sci.* **138**, 51367 (2021).

## ACKNOWLEDGEMENTS

This work is supported by the National Natural Science Foundation of China (No. 62101605), the Shenzhen Science and Technology Innovation Committee (No. JCYJ20190806145609284), the Fundamental Research Funds for the Central Universities, Sun Yat-sen University (Grant No. 22qntd1501). This work was partially carried out at the USTC Center for Micro and Nanoscale Research and Fabrication. Yuan Huang would like to acknowledge support from Zinergy Shenzhen Ltd.

## AUTHOR CONTRIBUTIONS

Y.H. and B.L. contributed equally to this work. Y.H. and B.L. conceived the idea and designed the experiments. B.L. carried out the fabrication of piezoresistive sensor and the performance measurement. W.Z. carried out the design of the signal management circuit system. G.Q. carried out the performance measurement of active powering senser integrated with a solid-state batteries. S.J., X.L., Z.N., and H.Z. participated in the discussion of the experimental data. Y.H. analyzed the experimental results and wrote the paper. H.Z. participated in the revision of the paper and supervised the research process.

## COMPETING INTERESTS

The authors declare no competing interests.

## ADDITIONAL INFORMATION

**Supplementary information** The online version contains supplementary material available at https://doi.org/10.1038/s41528-022-00226-z.

**Correspondence** and requests for materials should be addressed to Hang Zhou.

**Reprints and permission information** is available at http://www.nature.com/reprints

**Publisher's note** Springer Nature remains neutral with regard to jurisdictional claims in published maps and institutional affiliations.